

## Electroweak corrections to monojet production at the Tevatron and the LHC

ANSGAR DENNER<sup>1</sup>, STEFAN DITTMAYER<sup>2</sup>, TOBIAS KASPRZIK<sup>3</sup>, ALEXANDER MÜCK<sup>4</sup>

<sup>1</sup>*Universität Würzburg, Institut für Theoretische Physik und Astrophysik,  
D-97074 Würzburg, Germany*

<sup>2</sup>*Albert-Ludwigs-Universität Freiburg, Physikalisches Institut,  
D-79104 Freiburg, Germany*

<sup>3</sup>*Karlsruhe Institute of Technology (KIT), Institut für Theoretische Teilchenphysik,  
D-76128 Karlsruhe, Germany*

<sup>4</sup>*RWTH Aachen University, Institut für Theoretische Teilchenphysik und Kosmologie,  
D-52056 Aachen, Germany*

### **Abstract:**

Single-jet production with missing transverse momentum is one of the most promising discovery channels for new physics at the LHC. In the Standard Model, Z + jet production with a Z-boson decay into neutrinos leads to this monojet signature. To improve the corresponding Standard Model predictions, we present the calculation of the full next-to-leading-order (NLO) electroweak corrections and a recalculation of the NLO QCD corrections to monojet production at the Tevatron and the LHC. We discuss the phenomenological impact on the total cross sections as well as on relevant differential distributions.

# 1 Introduction

Many models for Beyond Standard Model (BSM) physics predict new particles which are not visible for a typical detector in a collider experiment. When such an invisible particle is produced and recoils against a QCD jet, the detector will measure a monojet event, i.e. an event which only shows a single jet with potentially large transverse momentum and an equal amount of missing transverse momentum. For instance, such monojet signatures are predicted in extra-dimension models, (see, e.g., Ref. [1]), where single (undetected) gravitons are produced together with hard jets (see Refs. [2, 3] for a next-to-leading-order (NLO) QCD analysis). Moreover, certain models including stable unparticles [4], as well as the decay of mini-black-holes, which might be produced at the LHC according to large-extra-dimension scenarios (see, e.g., Ref. [5] and references therein), may also give rise to single-jet events. Accordingly, it has been investigated how to discriminate the different models via their predicted phenomenological signatures at the LHC [6]. Recently, first experimental analyses of LHC monojet data have been accomplished [7, 8] to constrain the ADD model of Large Extra Dimensions [1] and to search for dark matter, finding agreement with the Standard Model (SM) predictions.

In the SM, monojets are produced in  $Z + \text{jet}$  events if the  $Z$  boson is decaying into neutrinos. Hence, any BSM search in the monojet channel relies on the precise predictions for this SM process. Moreover, monojet events from  $Z + \text{jet}$  production have a relatively large cross section and can be used to study the measurement of missing transverse momentum  $\cancel{p}_T$  in general. A proper understanding of missing transverse momentum  $\cancel{p}_T$  is relevant in an even wider class of BSM searches, in particular for searches in models containing a TeV-scale dark-matter candidate. As stated in Refs. [9, 10], for low values of  $\cancel{p}_T$ , uncertainties within the SM mostly arise from uncertainties in the jet-energy measurement. At high  $\cancel{p}_T$ , however, the SM background is indeed dominated by on-shell  $Z + \text{jet}$  production with the subsequent decay  $Z \rightarrow \nu_l \bar{\nu}_l$ . Of course, there are further sources for monojet events in the SM, for instance  $W + \text{jet}$  production, where the charged lepton from the  $W$ -boson decay is not reconstructed, which are not considered in this work.

BSM searches will probe monojets with larger and larger transverse momenta with increasing centre-of-mass (CM) energy and luminosity at the LHC. Since electroweak (EW) radiative corrections grow with energy and are known to reach tens of percent at the TeV scale, they become more and more relevant and cannot be neglected compared to the usually included corrections from strong interaction. For instance, in this paper we show that EW corrections reduce the SM monojet cross section by about 15% at a missing transverse momentum of only 500 GeV. Based on these motivations, in this work, we investigate in detail  $Z + \text{jet}$  production including the  $Z$ -boson decay into neutrinos, i.e.

$$pp/p\bar{p} \rightarrow Z + \text{jet} + X \rightarrow \nu_l \bar{\nu}_l + \text{jet} + X. \quad (1.1)$$

In particular, we provide the EW and QCD corrections at NLO not relying on any on-shell approximation for the intermediate  $Z$  boson.

From the QCD point of view, the description of  $Z + \text{jet}$  production with leptonically decaying  $Z$  bosons hardly depends on the specific final-state leptons in any order in perturbation theory, since the leptonic decay products are insensitive to strong contributions. For on-shell  $Z$  bosons, which appear, e.g., in the treatment via the narrow- $Z$ -width approximation, this means that the relative QCD corrections are indeed identical for  $Z(\rightarrow l^- l^+ / \nu_l \bar{\nu}_l) + \text{jet}$ . Including  $Z$ -boson off-shell effects, however, leads to differences between the two leptonic final states because of the different spin correlations due to the different chiral couplings of  $l$  and  $\nu_l$  and, more importantly the existence of  $\gamma^*$  exchange for charged leptons. The NLO corrections to  $Z + \text{jet}$  production

are known for a long time [11–13] and were matched with parton showers [14]. A resummation of large logarithms at the next-to-leading-logarithmic level was performed in Ref. [15] for vector-boson production at large transverse momentum.

Considering EW corrections, the situation is more involved, because of non-factorizable corrections due to interactions of initial-state partons and final-state leptons. In a first step, the purely weak one-loop corrections to  $Z$ +jet production in the SM were investigated in the on-shell approximation [16,17], i.e. with a stable external  $Z$  boson, and photonic corrections were ignored. For  $Z$  bosons at large transverse momentum, requiring a large CM energy, using on-shell  $Z$  bosons is a good approximation since the EW corrections are dominated by large universal Sudakov logarithms [18]. In Ref. [16] the leading corrections up to the next-to-leading logarithms at the one- and two-loop level were calculated. Later the full NLO weak corrections were added [17]. Although all off-shell effects are neglected, one would still expect the  $\cancel{p}_T$  distribution in the monojet scenario to be described well by the on-shell computation, at least at high energies. However, aiming at a precision at the percent level, photonic corrections have to be taken into account, as well as off-shell effects due to the decay of the virtual boson. These issues are resolved in this work for monojet production at the LHC and the Tevatron.

There are other uncertainties at the level of several percent affecting the cross section for monojet production that are not addressed in this work. These result, in particular, from missing higher-order QCD corrections, from the modelling of parton showers and fragmentation, from parton distribution functions (PDFs), and from the limited knowledge of the jet energy scale and resolution. Estimates on these uncertainties can be found in experimental publications on  $Z$ +jet production [19,20], in theory papers [21], and in discussions of PDF uncertainties [22]. These uncertainties will be further reduced by improved theoretical predictions and future experimental analyses. In the search for new physics in monojet production, the SM background cross section is typically estimated from experimental data for  $l^+l^-$ +jet events. In the analysis of Ref. [7], based on an integrated luminosity of  $33\text{ pb}^{-1}$ , the systematic uncertainties on the SM monojet event rates are at the level of 10% and result dominantly from limited statistics in the control region. With improved statistics the EW corrections may become even more important, in particular since many uncertainties cancel in the cross-section ratio of  $l^+l^-$ +jet and  $\nu_l\bar{\nu}_l$ +jet production.

Besides the new evaluation of the complete EW corrections for the off-shell case we have also recalculated the well-known NLO QCD corrections, supporting a phase-space dependent renormalization and factorization scale. Our results are implemented in a flexible Monte Carlo code that allows for the computation of total cross sections as well as differential distributions. Our implementation is completely generic in the sense that there are no restrictions for the event-selection criteria to be applied. All off-shell effects are included, and the finite  $Z$ -boson width is consistently taken care of using the complex-mass scheme [23]. Since the computation for the  $\nu_l\bar{\nu}_l$ +jet final state is closely related to the final state with two charged leptons, the presentation in this paper follows Ref. [24], where the calculation of the EW corrections to  $l^-l^+$ +jet production at hadron colliders was presented.

This paper is organized as follows. In Section 2, we briefly describe our calculation and discuss the relevant theoretical concepts. In Section 3, we specify the numerical input as well as the details of our event selection. Numerical results are given for monojet production both at the LHC and at the Tevatron. We present inclusive cross sections for specified sets of cuts and distributions for the jet transverse momentum and rapidity, as well as the missing transverse momentum, and discuss the impact of the EW contributions. Section 4 discusses a proper combination of the EW corrections with existing higher-order QCD predictions. We conclude in Section 5.

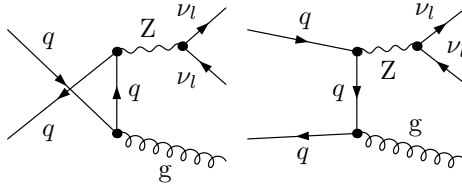


**Figure 1:** Feynman diagrams for the LO process (2.1).

## 2 Details of the calculation

This calculation closely follows the one for charged dilepton + jet production presented in Ref. [24]. Here we only briefly summarize the essential ingredients of our calculation and point to the differences with respect to Ref. [24]. More details can be found in Section 2 of that paper.

### 2.1 General setup

In the SM, at leading order (LO) in perturbation theory the transverse momentum of a single isolated jet is balanced by a Z boson, which decays into two undetected neutrinos. At hadron colliders, the partonic channels

$$q_i \bar{q}_i \rightarrow Z g \rightarrow \nu_l \bar{\nu}_l g, \quad (2.1)$$

$$q_i g \rightarrow Z q_i \rightarrow \nu_l \bar{\nu}_l q_i, \quad (2.2)$$

$$\bar{q}_i g \rightarrow Z \bar{q}_i \rightarrow \nu_l \bar{\nu}_l \bar{q}_i \quad (2.3)$$

have to be taken into account, where  $q_i$  denotes any light quark, i.e.  $q_i = u, d, c, s, b$ . Note that we always imply the summation over neutrino flavours in the final state, leading to a trivial factor of three for all cross sections compared to the cross sections for a single neutrino flavour. The tree-level Feynman diagrams for process (2.1) are shown in Figure 1. The intermediate Z-boson resonance is treated in a gauge-invariant way using the complex-mass scheme [23]. Since we consider Z + jet production with a subsequent Z-boson decay into neutrinos at NLO accuracy with respect to EW corrections, i.e. at the order  $\mathcal{O}(\alpha^3 \alpha_s)$ , we also include the photon-induced processes,

$$q_i \gamma \rightarrow Z q_i \rightarrow \nu_l \bar{\nu}_l q_i, \quad (2.4)$$

$$\bar{q}_i \gamma \rightarrow Z \bar{q}_i \rightarrow \nu_l \bar{\nu}_l \bar{q}_i, \quad (2.5)$$

which contribute at the order  $\mathcal{O}(\alpha^3)$  and may thus be relevant at the level of a few percent. The tree-level Feynman diagrams for process (2.4) can be found in Figure 2. We use the MRSTQED2004 set [25] of PDFs to estimate the photon content of the proton but employ modern PDF sets for all partonic channels without initial-state photons.

The Feynman diagrams and amplitudes are generated with the FEYNARTS package [26] and further processed with POLE [27] and FORMCALC [28], or alternatively with independent in-house *Mathematica* routines. Hence, all parts of the calculation are again performed in two independent ways with different tools.

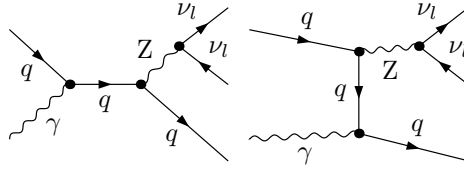


**Figure 2:** Feynman diagrams for the photon-induced process (2.4).

## 2.2 Virtual corrections

Virtual one-loop QCD and EW corrections are calculated for the partonic processes (2.1)–(2.3). We neglect the NLO QCD corrections to the photon-induced processes (2.4) and (2.5), which are expected to be as tiny as for  $W + \text{jet}$  production [29]. We also do not include the (loop-induced) contributions of the partonic process  $gg \rightarrow \nu_l \bar{\nu}_l g$  which can be estimated to be below one percent based on Ref. [13].

While the virtual QCD corrections consist of up to box (4-point) diagrams only, the more complicated NLO EW corrections, shown in Figure 3, involve also pentagon (5-point) diagrams (see Figure 4). As in our earlier work on  $l^+l^- + \text{jet}$  production, we follow the traditional Feynman-diagrammatic approach and evaluate tensor and scalar one-loop integrals (up to pentagon diagrams for the EW corrections) with complex masses using the methods and results of Refs. [30] and [31], respectively.

The partonic processes with (anti-)bottom quarks in the initial state involve massive top quarks in EW loop diagrams. These affect the total EW correction by about a permille for the most inclusive cross section discussed in Section 3 at the 14 TeV LHC and by even less at lower hadronic CM energy or at the Tevatron. For less inclusive cross sections when the EW Sudakov logarithms dominate at high partonic CM energy, the top mass does not play a role.

## 2.3 Real corrections

Compared to the  $l^+l^-$  final state discussed in Ref. [24], the EW corrections are substantially simpler, since final-state photon radiation off leptons is absent in the monojet production scenario. The emission of an additional photon in the partonic processes (2.1)–(2.3) leads to the processes

$$q_i \bar{q}_i \rightarrow \nu_l \bar{\nu}_l g \gamma, \quad (2.6)$$

$$q_i g \rightarrow \nu_l \bar{\nu}_l q_i \gamma, \quad (2.7)$$

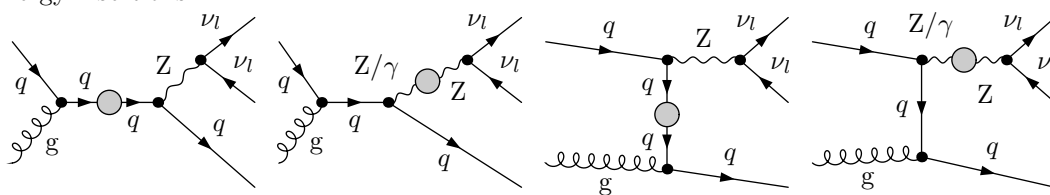
$$\bar{q}_i g \rightarrow \nu_l \bar{\nu}_l \bar{q}_i \gamma. \quad (2.8)$$

For the process (2.7) the relevant Feynman diagrams are listed in Figure 5. The corresponding amplitudes may be obtained from the amplitudes for the  $l^+l^- + \text{jet} + \gamma$  final state by switching off the virtual photon as well as the final-state radiation off the leptons. In addition one has to replace the  $Zl^-l^+$  coupling by the  $Z\nu_l\bar{\nu}_l$  coupling.

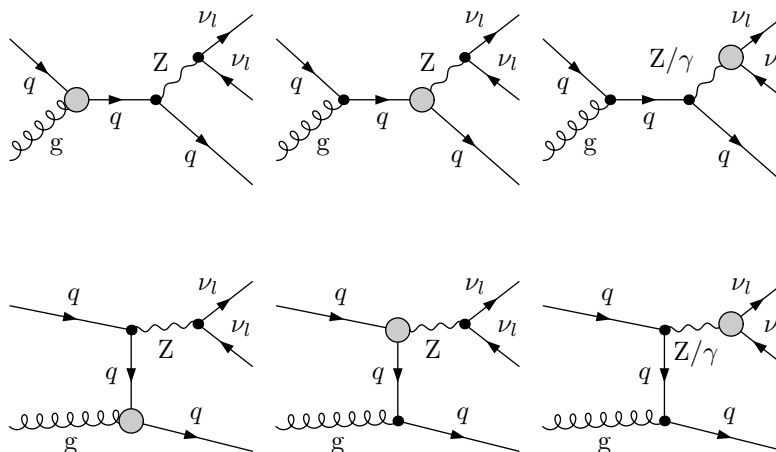
In order to treat the soft and collinear singularities in an efficient way we use the dipole subtraction formalism as specified for photon emission in Refs. [32, 33].

As in all processes with jets in the final state, the inclusion of EW corrections to monojet production asks for a precise event definition in order to distinguish single-jet from single-photon production. We follow the strategy used for  $\nu_l l^+ + \text{jet}$  and  $l^- l^+ + \text{jet}$  production which is detailed in Refs. [24, 29, 34]: We exclude jets which primarily consist of a hard photon (see Section 3)

Self-energy insertions:



Triangle insertions:



Box and pentagon insertions:

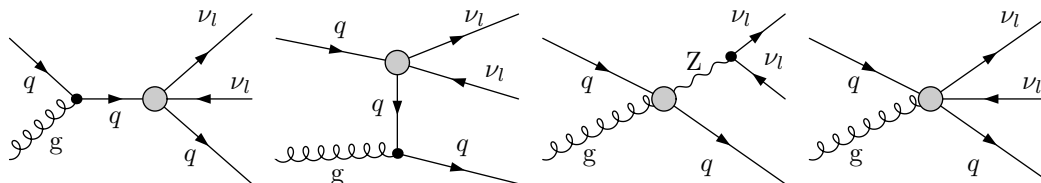


**Figure 3:** Contributions of different one-particle irreducible vertex functions (indicated as blobs) to the LO process (2.2); there are contributions from self-energies, triangles, boxes, and pentagon graphs.

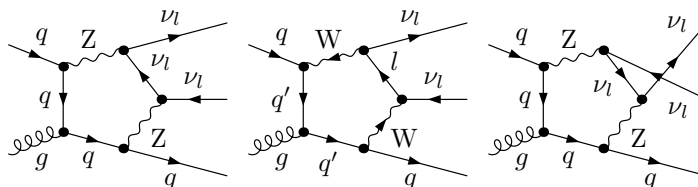


**Figure 4:** Virtual pentagon contributions to the process (2.2). Note that for external bottom quarks the exchange of two W bosons leads to diagrams with massive top-quark lines ( $q' = \text{top}$ ) in the loop.

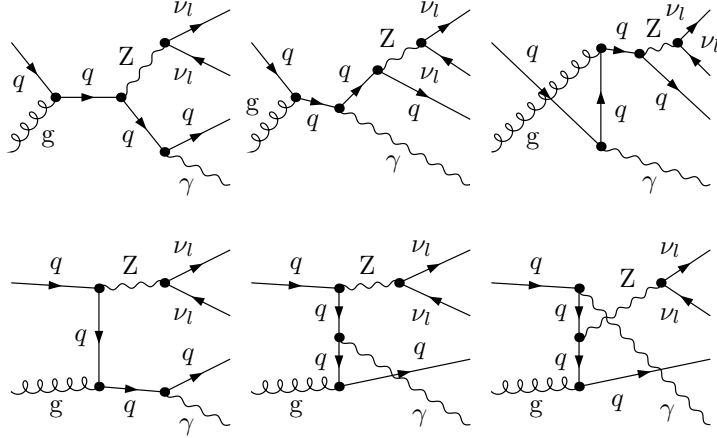


**Figure 5:** Real photonic bremsstrahlung corrections to the LO process (2.2).

and capture the non-perturbative physics in the collinear quark–photon splittings [35] by means of the measured fragmentation function [36]. The error on our predictions associated to the uncertainties in the fragmentation function are negligible.

The calculation of the QCD corrections to single-jet production is completely analogous to dilepton + jet production and has been discussed in Section 2.3 of Ref. [24]. It contains a plethora of partonic channels (see Eqs. (2.11)–(2.21) in Ref. [24]), in particular involving six-fermion processes with a rich flavour structure of the involved (anti-)quarks. For six-fermion processes with identical quarks, again, we do not consider interference contributions between purely electroweak diagrams and gluon-exchange diagrams which enter at order  $\mathcal{O}(\alpha^3\alpha_s)$ . These contributions are colour-suppressed and do not exhibit any further enhancement. Thus, they only lead to tiny corrections, as has been demonstrated in Ref. [29].

### 3 Numerical results

#### 3.1 Input parameters and setup

The relevant SM input parameters are

$$\begin{aligned}
 G_\mu &= 1.16637 \times 10^{-5} \text{ GeV}^{-2}, & \alpha_s(M_Z) &= 0.1202, \\
 M_W^{\text{OS}} &= 80.398 \text{ GeV}, & \Gamma_W^{\text{OS}} &= 2.141 \text{ GeV}, \\
 M_Z^{\text{OS}} &= 91.1876 \text{ GeV}, & \Gamma_Z^{\text{OS}} &= 2.4952 \text{ GeV}, \\
 M_H &= 120 \text{ GeV}, & m_t &= 172.6 \text{ GeV},
 \end{aligned} \tag{3.1}$$

which essentially follow Ref. [37]. To facilitate comparisons, we stick to the input parameters used in Refs. [24, 29] for the analysis of  $\nu_l l^+ + \text{jet}$  and  $l^+ l^- + \text{jet}$  production, respectively. The numerical results presented in this paper will only change marginally using up-to-date values of  $M_W$ ,  $M_H$ , and  $m_t$ . The CKM matrix only appears in loops and is set to unity, because its effect is negligible.

As in our earlier work on  $V + \text{jet}$  production, using the complex-mass scheme [23], we convert the “on-shell” (OS) values of  $M_V^{\text{OS}}$  and  $\Gamma_V^{\text{OS}}$  ( $V = W, Z$ ) into the “pole values” [38] and use the corresponding numerical values

$$\begin{aligned} M_W &= 80.370 \dots \text{ GeV}, & \Gamma_W &= 2.1402 \dots \text{ GeV}, \\ M_Z &= 91.153 \dots \text{ GeV}, & \Gamma_Z &= 2.4943 \dots \text{ GeV} \end{aligned} \quad (3.2)$$

in the numerics. However, using  $M_V^{\text{OS}}$  instead would be hardly visible in the results. We again adopt the  $G_\mu$  scheme so that the results are practically independent of the light fermion masses.

We use the central MSTW2008NLO PDF set [39] and the  $\alpha_s$  running from the LHAPDF collaboration [40] (implying  $\alpha_s(M_Z)$  given in (3.1)). Only the photon-induced processes are evaluated with the MRSTQED2004 set of PDFs [25] (implying  $\alpha_s(M_Z) = 0.1190$ ).

Numerical results are presented for the identified QCD and QED factorization scales and the QCD renormalization scale  $\mu = M_Z$  or the phase-space-dependent scale

$$\mu^{\text{var}} = \sqrt{M_Z^2 + (p_T^{\text{had}})^2}, \quad (3.3)$$

where  $p_T^{\text{had}}$  is given by the  $p_T$  of the summed four-momenta of all partons (quarks and/or gluons) in the final state, which is more adequate for high- $p_T$  jets (see discussion in Ref. [24] or Ref. [41]).

## 3.2 Phase-space cuts and event selection

We define the monojet signature by the recombination procedure for quarks, gluons, and photons into jets and the basic cuts discussed in the following subsections.

### 3.2.1 Recombination

To define the recombination procedure and the separation cuts, we use the variables  $R_{ij} = \sqrt{(y_i - y_j)^2 + \phi_{ij}^2}$ , where  $y_i$  denotes the rapidity  $y_i = \frac{1}{2} \ln[(E + p_L)/(E - p_L)]$  of particle  $i$  and  $\phi_{ij}$  is the azimuthal angle in the transverse plane between the particles  $i$  and  $j$ . In the definition of the rapidity,  $E$  denotes the particle’s energy and  $p_L$  its three-momentum along the beam axis. The recombination procedure, where we simply add four-momenta to form a pseudo-particle, works as follows:

1. A photon and a parton  $a$  (quark or gluon) are recombined for  $R_{\gamma a} < 0.5$ . The energy fraction of the photon inside the jet  $z_\gamma = E_\gamma/(E_\gamma + E_a)$  is used to distinguish between single-jet and single-photon production (using quark-to-photon fragmentation functions to describe the non-perturbative collinear splitting). For  $z_\gamma > 0.7$  the event is rejected. Our results are not very sensitive to the specific choice of the cut on  $z_\gamma$ .
2. Two partons  $a, b$  are recombined for  $R_{ab} < 0.5$ . For our simple final-state configurations, this procedure is equivalent to the Tevatron Run II  $k_T$  algorithm [42], the anti- $k_T$  algorithm [43], and similar algorithms for jet reconstruction with resolution parameter  $D = 0.5$ .

### 3.2.2 Basic cuts

After applying the recombination procedure of the previous section we define monojet events by the following basic cuts:

1. A partonic object (after a possible recombination) is called a jet if its transverse momentum  $p_T$  is larger than  $p_{T,\text{jet}}^{\text{cut}} = 25 \text{ GeV}$ . Events are required to include at least one jet.
2. We demand a missing transverse momentum (i.e. the transverse momentum of the neutrino pair)  $\cancel{p}_T > 25 \text{ GeV}$ . Of course, at LO this requirement is automatically fulfilled, since the virtual Z and the jet are always back-to-back.
3. The events have to be central, i.e. the jet has to be produced in the rapidity range  $|y| < y_{\text{max}} = 2.5$ .
4. To suppress background from a mis-measurement of the transverse momentum of one of the jets in events with two hard back-to-back jets, which also lead to a signature with missing momentum, we require a separation of a jet and the missing momentum  $\cancel{p}_T$  in the transverse plane. As proposed in Ref. [7], we discard events with  $\phi_{jZ} < 0.5$ , where  $\phi_{jZ}$  is the angle between  $p_{T,\text{jet}}$  and  $\cancel{p}_T$ . A similar separation cut could be applied for the photon and  $\cancel{p}_T$ . However, we have checked that such a separation only insignificantly changes the numerical results.

Additionally, we present results obtained by applying an explicit veto against a second hard jet with  $p_T > p_{T,j1}/2$ , where  $p_{T,j1}$  denotes the  $p_T$  of the “leading” jet, i.e. the one with maximal  $p_T$ . This two-jet veto reduces the relative QCD corrections and moreover enforces the kinematic structure of monojet events, i.e. the transverse momentum of the hard jet is to be (mainly) balanced by missing transverse momentum and not by a second hard jet (see discussion below).

### 3.3 Results on cross sections and distributions

Numerical results are presented for the production of a neutrino pair in association with a jet at the Tevatron ( $p\bar{p}$  collisions with a CM energy of  $\sqrt{s} = 1.96 \text{ TeV}$ ) and at the LHC. For the latter, we show results for  $pp$  collisions at  $\sqrt{s} = 8 \text{ TeV}$ , corresponding to the available energy in the year 2012, as well as  $\sqrt{s} = 14 \text{ TeV}$ , the design energy of the LHC.

#### 3.3.1 Overview of cross-section predictions

We present the LO cross section  $\sigma_0$  and corrections  $\delta$ , defined relative to the LO cross section by  $\sigma = \sigma_0 \times (1 + \delta)$ . The EW corrections are labelled  $\delta_{\text{EW}}^{\mu=M_Z}$  or  $\delta_{\text{EW}}^{\text{var}}$  indicating a fixed scale choice or the phase-space dependent scale choice as specified in (3.3), respectively. For the EW corrections the difference is small, as expected, while for the QCD part a sensible scale choice is crucial as discussed below.

As already observed in  $W + \text{jet}$  and  $l^-l^+ + \text{jet}$  production in Refs. [24, 29] and shown for  $\nu_l\bar{\nu}_l + \text{jet}$  below, the QCD corrections become larger and larger with increasing  $p_T$  of the leading jet due to dijet kinematics where one of the quark lines radiates a relatively soft Z boson. The cut on  $\phi_{jZ}$ , discussed in Section 3.2.2, partly removes these configurations. However, a usual cut value like  $\phi_{jZ} < 0.5$  is too small to avoid the problem. This part of the cross section does not really correspond to a true NLO correction to single-jet production. It even contradicts the intuitive understanding how a monojet event looks like. Fortunately, it can be easily separated employing the veto introduced at the end of Section 3.2.2. This particular jet veto yields a sensible definition of monojet events since it is equivalent to raising the required amount of missing transverse momentum along with the transverse momentum of the observed leading jet. NLO QCD corrections with a jet veto ( $\delta_{\text{QCD,veto}}^{\mu=M_Z}$ ,  $\delta_{\text{QCD,veto}}^{\text{var}}$ ) and without a jet veto ( $\delta_{\text{QCD}}^{\mu=M_Z}$ ,  $\delta_{\text{QCD}}^{\text{var}}$ ) are presented below to demonstrate the importance of the jet veto.

pp  $\rightarrow \nu_l \bar{\nu}_l$  jet + X at  $\sqrt{s} = 14$  TeV

$p_{T,\text{jet}}/\text{GeV}$	25 – $\infty$	50 – $\infty$	100 – $\infty$	200 – $\infty$	500 – $\infty$	1000 – $\infty$
$\sigma_0^{\mu=M_Z}/\text{pb}$	1627.25(3)	582.66(3)	125.669(5)	15.0488(5)	0.40302(1)	0.0121944(2)
$\sigma_0^{\text{var}}/\text{pb}$	1608.99(2)	566.52(2)	116.092(4)	12.2928(4)	0.243365(6)	0.00523456(9)
$\delta_{\text{EW}}^{\mu=M_Z}/\%$	0.0	–0.4	–2.1	–6.5	–16.7	–27.6(1)
$\delta_{\text{EW}}^{\text{var}}/\%$	0.0	–0.4	–2.0	–6.2	–16.1	–26.6(1)
$\delta_{\text{QCD}}^{\mu=M_Z}/\%$	8.5	38.5(1)	51.8(1)	76.2(1)	126.4(1)	179.3(1)
$\delta_{\text{QCD}}^{\text{var}}/\%$	8.4	39.7(1)	57.8(1)	97.2(1)	210.5(1)	397.3(1)
$\delta_{\text{QCD,veto}}^{\mu=M_Z}/\%$	–8.8	6.9(1)	7.1(1)	–0.2(1)	–31.4(1)	–68.9(1)
$\delta_{\text{QCD,veto}}^{\text{var}}/\%$	–8.0	9.6(1)	14.9(1)	20.2(1)	21.0(1)	23.4(1)
$\delta_{\gamma}^{\mu=M_Z}/\%$	0.0	0.1	0.1	0.1	0.1	0.2
$\delta_{\gamma}^{\text{var}}/\%$	0.0	0.1	0.1	0.1	0.2	0.5
$\sigma_{\text{full,veto}}^{\text{var}}/\text{pb}$	1480.7(2)	619.2(3)	131.23(5)	14.029(6)	0.2557(1)	0.005090(3)

**Table 1:** Integrated cross sections for different cuts on the  $p_T$  of the leading jet (jet with highest  $p_T$ ) at the LHC with  $\sqrt{s} = 14$  TeV. We show the LO results both for a variable and for a constant scale along with the corresponding EW corrections  $\delta_{\text{EW}}$ , the QCD corrections  $\delta_{\text{QCD}}$  with or without employing a veto on a second hard jet, and the corrections due to photon-induced processes  $\delta_{\gamma}$ . Finally, we show the full NLO cross section  $\sigma_{\text{full,veto}}^{\text{var}}$  for which all the corrections are added to the LO results for a variable scale. The error from the Monte Carlo integration for the last digit(s) is given in parenthesis as far as significant.

The impact  $\delta_{\gamma}$  of the photon-induced tree-level processes (2.4) and (2.5) is shown relative to the LO cross section at  $\mathcal{O}(\alpha^2\alpha_s)$  without initial-state photons.

In Tables 1–6 we summarize our results for LO integrated cross sections and the corresponding relative corrections for different cuts on the transverse momentum of the leading jet and the missing transverse momentum. All other cuts and the corresponding event selection follow our default choice as introduced in Section 3.2. In Figures 6–8 we present the corresponding results for differential distributions. Both, in the tables and the figures we also show the NLO cross section  $\sigma_{\text{full,veto}}^{\text{var}}$  including the EW corrections, the photon-induced processes, and the QCD corrections with the jet veto for the variable scale choice. All results are discussed in detail in the following subsections.

### 3.3.2 Transverse momentum and rapidity of the leading jet

Tables 1–3 show the predictions for different cuts on the transverse momentum of the leading jet,  $p_{T,\text{jet}}$ , at the LHC and the Tevatron. The corresponding differential cross sections are displayed in Figure 6 for the LHC with  $\sqrt{s} = 14$  TeV and the Tevatron. The qualitative features of the EW corrections are similar to the results obtained earlier for  $l^+l^-$  + jet production.

pp  $\rightarrow \nu_l \bar{\nu}_l$  jet + X at  $\sqrt{s} = 8$  TeV

$p_{T,\text{jet}} / \text{GeV}$	25 – $\infty$	50 – $\infty$	100 – $\infty$	200 – $\infty$	500 – $\infty$	1000 – $\infty$
$\sigma_0^{\mu=M_Z} / \text{pb}$	782.38(1)	263.82(1)	50.954(2)	4.9461(2)	0.075842(2)	0.00086825(2)
$\sigma_0^{\text{var}} / \text{pb}$	768.26(1)	252.79(1)	45.631(2)	3.8100(1)	0.0409508(8)	0.0003054(3)
$\delta_{\text{EW}}^{\mu=M_Z} / \%$	0.1	-0.3	-2.0	-6.2	-16.1	-26.9(1)
$\delta_{\text{EW}}^{\text{var}} / \%$	0.1	-0.3	-1.8	-5.9	-15.5	-25.8(1)
$\delta_{\text{QCD}}^{\mu=M_Z} / \%$	8.2	33.6(1)	41.5(1)	58.0(1)	97.2(1)	151.7(1)
$\delta_{\text{QCD}}^{\text{var}} / \%$	8.8	36.6(1)	51.5(1)	87.6(1)	203.7(1)	444.7(1)
$\delta_{\text{QCD,veto}}^{\mu=M_Z} / \%$	-7.0	5.4(1)	2.0(1)	-8.7(1)	-39.2(1)	-78.1(1)
$\delta_{\text{QCD,veto}}^{\text{var}} / \%$	-5.6	9.5(1)	13.1(1)	17.5(1)	24.8(1)	35.5(1)
$\delta_{\gamma}^{\mu=M_Z} / \%$	0.1	0.1	0.1	0.1	0.2	0.4
$\delta_{\gamma}^{\text{var}} / \%$	0.1	0.1	0.1	0.2	0.4	1.0
$\sigma_{\text{full,veto}}^{\text{var}} / \text{pb}$	726.04(7)	276.4(1)	50.82(2)	4.260(2)	0.04491(3)	0.0003381(3)

**Table 2:** Integrated cross sections for different cuts on the  $p_T$  of the leading jet at the LHC with  $\sqrt{s} = 8$  TeV. See also caption of Table 1.

p $\bar{p} \rightarrow \nu_l \bar{\nu}_l$  jet + X at  $\sqrt{s} = 1.96$  TeV

$p_{T,\text{jet}} / \text{GeV}$	25 – $\infty$	50 – $\infty$	75 – $\infty$	100 – $\infty$	200 – $\infty$	300 – $\infty$
$\sigma_0^{\mu=M_Z} / \text{pb}$	96.613(2)	24.721(1)	8.1060(4)	3.0539(1)	0.131732(5)	0.0095024(6)
$\sigma_0^{\text{var}} / \text{pb}$	93.800(2)	23.027(1)	7.1807(3)	2.5642(1)	0.090028(4)	0.0054067(4)
$\delta_{\text{EW}}^{\mu=M_Z} / \%$	0.2	0.0	-0.6	-1.3	-4.5	-7.4
$\delta_{\text{EW}}^{\text{var}} / \%$	0.2	0.0	-0.5	-1.2	-4.0	-6.6
$\delta_{\text{QCD}}^{\mu=M_Z} / \%$	9.9	19.2(1)	12.9(1)	7.0(1)	-16.1(1)	-38.6(1)
$\delta_{\text{QCD}}^{\text{var}} / \%$	11.8	25.1(1)	24.0(1)	23.9(1)	24.7(1)	24.9(1)
$\delta_{\text{QCD,veto}}^{\mu=M_Z} / \%$	2.0	4.1(1)	-2.6(1)	-9.6(1)	-34.4(1)	-56.5(3)
$\delta_{\text{QCD,veto}}^{\text{var}} / \%$	4.3	10.6(1)	8.8(1)	7.6(1)	3.9(1)	2.1(1)
$\delta_{\gamma}^{\mu=M_Z} / \%$	0.1	0.1	0.1	0.1	0.1	0.1
$\delta_{\gamma}^{\text{var}} / \%$	0.1	0.1	0.1	0.1	0.2	0.2
$\sigma_{\text{full,veto}}^{\text{var}} / \text{pb}$	98.074(9)	25.49(1)	7.781(7)	2.732(1)	0.0901(1)	0.005175(5)

**Table 3:** Integrated cross sections for different cuts on the  $p_T$  of the leading jet at the Tevatron. See also caption of Table 1.

pp  $\rightarrow \nu_l \bar{\nu}_l$  jet + X at  $\sqrt{s} = 14$  TeV

$\cancel{p}_T$ / GeV	25 – $\infty$	50 – $\infty$	100 – $\infty$	200 – $\infty$	500 – $\infty$	1000 – $\infty$
$\sigma_0^{\mu=M_Z}$ / pb	1627.25(3)	582.66(3)	125.669(5)	15.0488(5)	0.40302(1)	0.0121944(2)
$\sigma_0^{\text{var}}$ / pb	1608.99(2)	566.52(2)	116.092(4)	12.2928(4)	0.243365(6)	0.00523456(9)
$\delta_{\text{EW}}^{\mu=M_Z}$ / %	0.0	-0.3	-2.0	-6.3	-16.5	-27.4(1)
$\delta_{\text{EW}}^{\text{var}}$ / %	0.0	-0.2	-1.8	-5.9	-15.8	-26.2(1)
$\delta_{\text{QCD}}^{\mu=M_Z}$ / %	8.5	48.1(1)	48.3(1)	35.5(1)	-2.6(1)	-44.2(1)
$\delta_{\text{QCD}}^{\text{var}}$ / %	8.4	48.4(1)	51.1(1)	47.6(1)	40.4	38.5
$\delta_{\text{QCD,veto}}^{\mu=M_Z}$ / %	-8.8	18.8(1)	16.5(1)	5.6(1)	-27.9(1)	-64.4(1)
$\delta_{\text{QCD,veto}}^{\text{var}}$ / %	-8.0	20.9(1)	22.6(1)	22.8(1)	21.6(1)	24.3
$\delta_{\gamma}^{\mu=M_Z}$ / %	0.0	0.1	0.1	0.1	0.1	0.2
$\delta_{\gamma}^{\text{var}}$ / %	0.0	0.1	0.1	0.1	0.2	0.5
$\sigma_{\text{full,veto}}^{\text{var}}$ / pb	1480.7(2)	683.9(2)	140.37(4)	14.388(4)	0.2581(1)	0.005161(3)

**Table 4:** Integrated cross sections for different cuts on the missing  $p_T$  at the LHC with  $\sqrt{s} = 14$  TeV. See also caption of Table 1.

pp  $\rightarrow \nu_l \bar{\nu}_l$  jet + X at  $\sqrt{s} = 8$  TeV

$\cancel{p}_T$ / GeV	25 – $\infty$	50 – $\infty$	100 – $\infty$	200 – $\infty$	500 – $\infty$	1000 – $\infty$
$\sigma_0^{\mu=M_Z}$ / pb	782.38(1)	263.82(1)	50.954(2)	4.9461(2)	0.075842(2)	0.00086825(2)
$\sigma_0^{\text{var}}$ / pb	768.26(1)	252.79(1)	45.631(2)	3.8100(1)	0.0409508(8)	0.0003054(3)
$\delta_{\text{EW}}^{\mu=M_Z}$ / %	0.1	-0.2	-1.8	-6.0	-15.8	-26.6(1)
$\delta_{\text{EW}}^{\text{var}}$ / %	0.1	-0.1	-1.6	-5.6	-15.1	-25.2(1)
$\delta_{\text{QCD}}^{\mu=M_Z}$ / %	8.2	43.7(1)	39.9(1)	25.3(1)	-12.4(1)	-57.2(1)
$\delta_{\text{QCD}}^{\text{var}}$ / %	8.8	45.8(1)	46.7(1)	44.8(1)	43.4	47.1
$\delta_{\text{QCD,veto}}^{\mu=M_Z}$ / %	-7.0	16.9(1)	10.8(1)	-1.4(1)	-33.5(1)	-72.7(1)
$\delta_{\text{QCD,veto}}^{\text{var}}$ / %	-5.6	20.5(1)	20.5(1)	22.4(1)	27.3	35.8(1)
$\delta_{\gamma}^{\mu=M_Z}$ / %	0.1	0.1	0.1	0.1	0.2	0.4
$\delta_{\gamma}^{\text{var}}$ / %	0.1	0.1	0.1	0.2	0.4	1.0
$\sigma_{\text{full,veto}}^{\text{var}}$ / pb	726.04(7)	304.53(9)	54.29(1)	4.457(1)	0.04611(1)	0.0003407(2)

**Table 5:** Integrated cross sections for different cuts on the missing  $p_T$  at the LHC with  $\sqrt{s} = 8$  TeV. See also caption of Table 1.

$p\bar{p} \rightarrow \nu_l \bar{\nu}_l \text{ jet} + X$  at  $\sqrt{s} = 1.96$  TeV

$p_{\text{T}}/\text{GeV}$	25 – $\infty$	50 – $\infty$	75 – $\infty$	100 – $\infty$	200 – $\infty$	300 – $\infty$
$\sigma_0^{\mu=M_Z}/\text{pb}$	96.613(2)	24.721(1)	8.1060(4)	3.0539(1)	0.131732(5)	0.0095024(6)
$\sigma_0^{\text{var}}/\text{pb}$	93.800(2)	23.027(1)	7.1807(3)	2.5642(1)	0.090028(4)	0.0054067(4)
$\delta_{\text{EW}}^{\mu=M_Z}/\%$	0.2	0.2	−0.4	−1.1	−4.2	−7.0
$\delta_{\text{EW}}^{\text{var}}/\%$	0.2	0.2	−0.2	−0.8	−3.5	−6.0
$\delta_{\text{QCD}}^{\mu=M_Z}/\%$	9.9	38.1	31.5	25.2	2.1	−16.9
$\delta_{\text{QCD}}^{\text{var}}/\%$	11.8	43.6	41.3	39.6	35.6	34.8
$\delta_{\text{QCD,veto}}^{\mu=M_Z}/\%$	2.0	20.0	10.7	5.9	−12.5	−28.3
$\delta_{\text{QCD,veto}}^{\text{var}}/\%$	4.3	26.4	21.7	21.8	23.1	25.5
$\delta_{\gamma}^{\mu=M_Z}/\%$	0.1	0.1	0.1	0.1	0.1	0.1
$\delta_{\gamma}^{\text{var}}/\%$	0.1	0.1	0.1	0.1	0.2	0.2
$\sigma_{\text{full,veto}}^{\text{var}}/\text{pb}$	98.074(9)	29.178(4)	8.729(2)	3.1058(5)	0.10782(2)	0.006474(1)

**Table 6:** Integrated cross sections for different cuts on the missing  $p_{\text{T}}$  at the Tevatron with  $\sqrt{s} = 1.96$  TeV. See also caption of Table 1.

At high CM energies the generic well-known (negative) Sudakov logarithms of the form  $\ln^2(\hat{s}/M_Z^2)$  in the virtual EW corrections lead to large corrections, e.g.  $-25\%$  for  $p_{\text{T,jet}} \sim 1$  TeV. If the integrated cross section is not dominated by events with high CM energy (left columns in the tables) the EW corrections for monojet production are negligibly small, at the permille level. As expected, the relative EW corrections are neither particularly sensitive to the scale choice nor to the CM energy of the LHC. Also at the Tevatron, the qualitative features of the corrections are very similar. The onset of the Sudakov dominance is visible as can be seen in Table 3 and Figure 6. However, owing to the limited kinematic reach of the Tevatron the effects are not very pronounced.

The dominating Sudakov logarithms lead to corrections to the underlying process of Z + jet production and do not depend on the specific decay channel. Hence, the similarity of the large EW corrections presented here with the EW corrections to  $l^+l^- + \text{jet}$  production presented in Ref. [24] is not surprising. At large  $p_{\text{T,jet}}$  the corrections differ only at the level of 1%. Given this fact, also the agreement with earlier on-shell calculations Refs. [16, 17] within 1–2% observed before still holds (see Figure 5 in Ref. [17]). In other words, it is well justified to use the Sudakov approximation to reliably predict the transverse-momentum distribution of this very observable. The residual differences at the 1% level, which might be of interest for a precision determination of cross-section ratios for different Z-boson decay modes, are discussed in detail in Section 3.3.4.

The contribution  $\delta_{\gamma}$  from the photon-induced processes are tiny and do not reach the percent level even for large cut values. This indeed justifies to safely neglect the NLO QCD corrections to the photon-induced channels.

Turning to the NLO QCD results at the LHC at 14 TeV, we observe results similar to  $l^+l^- + \text{jet}$  production presented in Ref. [24]. From the QCD point of view, the corrections to

$l^+l^- + \text{jet}$  production and  $\nu_l\bar{\nu}_l + \text{jet}$  production are almost equivalent. However, the acceptance and isolation cuts necessarily differ and can lead to quantitatively different corrections while the qualitative picture is similar. The corrections turn out to be accidentally small ( $\sim 10\%$ ) for our default cuts in the monojet case. As discussed above, the cross section for large cut values of  $p_{T,\text{jet}}$  contains large contributions from two-jet events with relatively little missing transverse momentum, i.e. events having little in common with typical monojet events but resulting in huge positive corrections. The correction  $\delta_{\text{QCD}}^{\mu=M_Z}$  is smaller than  $\delta_{\text{QCD}}^{\text{var}}$ , because it is defined relative to a larger LO cross section. In absolute size, however, the two NLO corrections are similar. Using the jet veto proposed at the end of Section 3.2.2, the corrections are reduced, and  $\delta_{\text{QCD}}^{\text{var}}$  only rises to the 20% level for large cut values at the 14 TeV LHC. As expected, at large  $p_{T,\text{jet}}$ , the overestimated LO cross section with a fixed scale receives large negative corrections and the discrepancy of the LO results for the two scale choices is largely removed by including the NLO corrections.

At CM energy  $\sqrt{s} = 8 \text{ TeV}$  (see Table 2) and at the Tevatron (see Table 3), the same qualitative results are found. Using the variable scale, increasingly negative corrections with increasing  $p_{T,\text{jet}}$  can be avoided, in particular when employing a jet veto, and stable results are obtained. At the Tevatron, the jet veto is not as important because of its kinematical limitations.

Concerning the rapidity of the leading jet  $y_{\text{jet}}$  displayed in Figure 7, the EW corrections both at the LHC and the Tevatron are flat and extremely small in size, resembling the corrections to the total cross sections. At the LHC, the QCD corrections are positive (about 8%) and give rise to nearly constant  $K$ -factors in the whole rapidity range. Introducing a dedicated two-jet veto, as detailed above, shifts the relative corrections to the level of  $-10\%$ . At the Tevatron, the effect of the jet veto turns out to be smaller than at the LHC, whereas the scale dependence is somewhat larger.

### 3.3.3 Missing transverse momentum

The missing transverse momentum, i.e. the transverse momentum of the Z boson, equals the leading-jet  $p_T$  at LO, while at NLO the two observables become different if an additional bremsstrahlung particle is present. The relative EW corrections for different cut values of  $p_T$  in Tables 4–6 as well as the relative corrections to the differential distributions presented in Figure 8 are completely dominated by virtual contributions and, hence, hardly differ from the corresponding values in Tables 1–3 and Figure 6, respectively. In contrast, the nature of the corresponding QCD corrections changes dramatically. The huge positive corrections at high  $p_{T,\text{jet}}$  induced by events with two hard back-to-back jets are absent, since now a large missing momentum has to be balanced such that back-to-back jets are kinematically suppressed. Therefore, the two-jet veto only slightly changes the corresponding relative corrections. If a two-jet veto is applied, the missing transverse momentum has to be balanced by one hard jet, leading to similar values of  $p_{T,\text{jet}}$  and  $p_T$  for such events. Therefore, at the LHC the relative QCD corrections are very similar for both observables at large  $p_T$ , since events with two hard jets emitted in the same direction are rare. Note in addition that the variable-scale choice leads to almost constant  $K$ -factors for QCD corrections both at the LHC and the Tevatron for the corresponding distributions (Figure 8).

### 3.3.4 Comparison of EW corrections for different leptonic Z-boson decays

In this section, we compare the EW corrections for Z + jet production with a subsequent Z-boson decay into charged leptons, as investigated in detail in Ref. [24], with the prediction for the monojet signature. As we have discussed before, due to the dominant universal Sudakov logarithms the EW corrections are very similar in the high-energy tails of distributions where

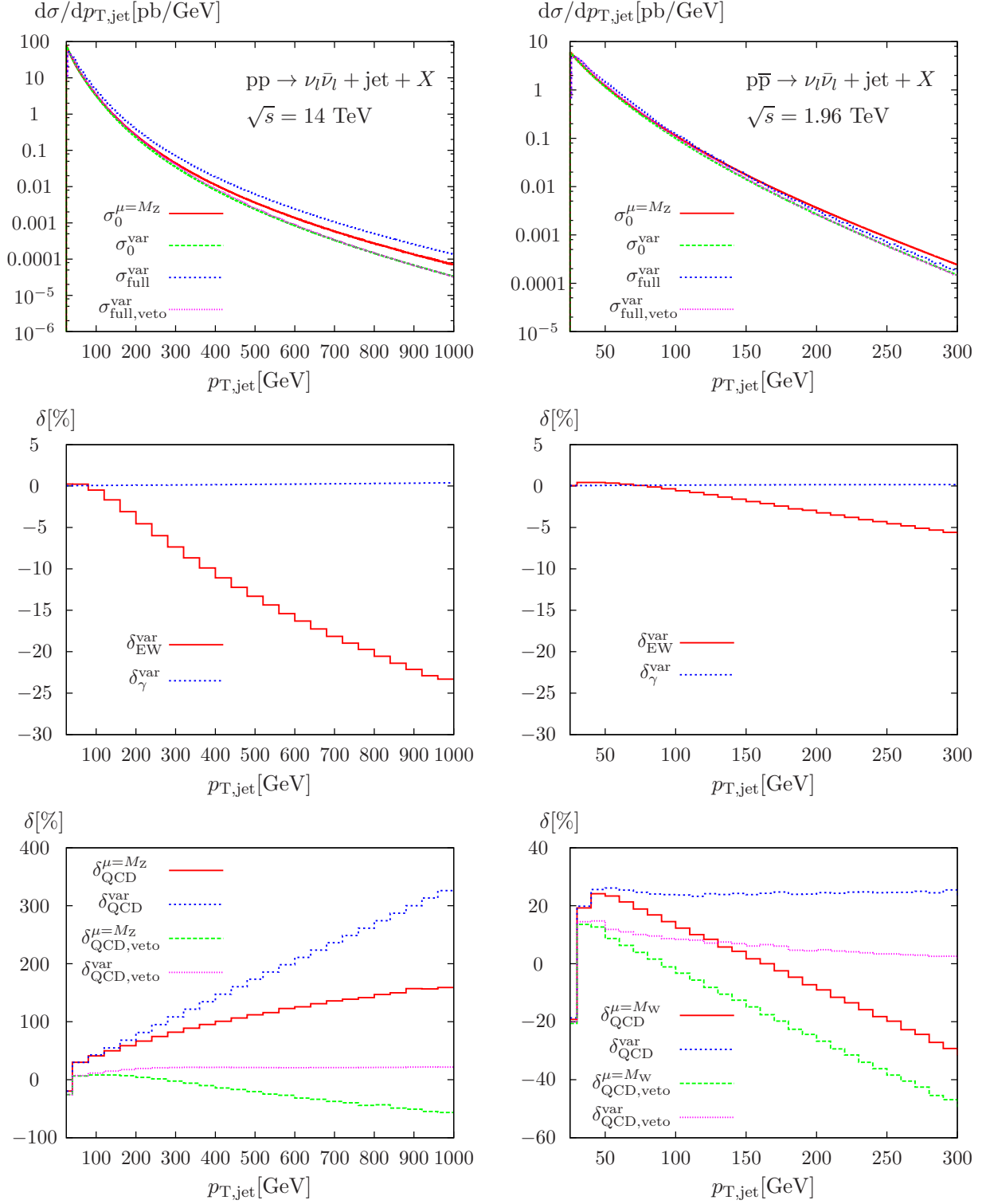


**Figure 6:** LO and fully corrected distribution (top), corresponding relative EW and photon-induced corrections (middle), and relative QCD corrections (bottom) for the transverse momentum of the leading jet at the LHC (left) and the Tevatron (right).

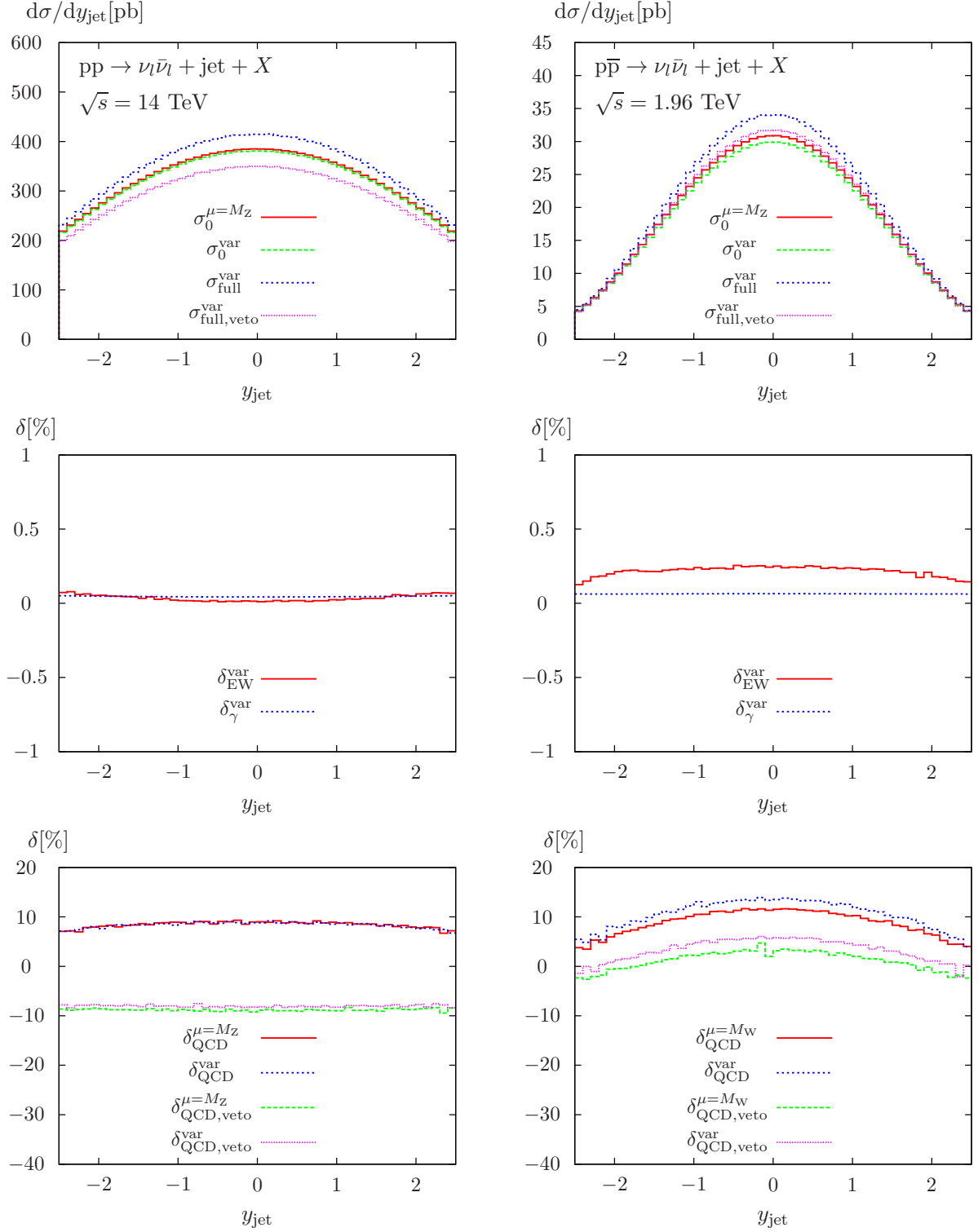


**Figure 7:** LO and fully corrected distribution (top), corresponding relative EW and photon-induced corrections (middle), and relative QCD corrections (bottom) for the rapidity of the leading jet at the LHC (left) and the Tevatron (right).

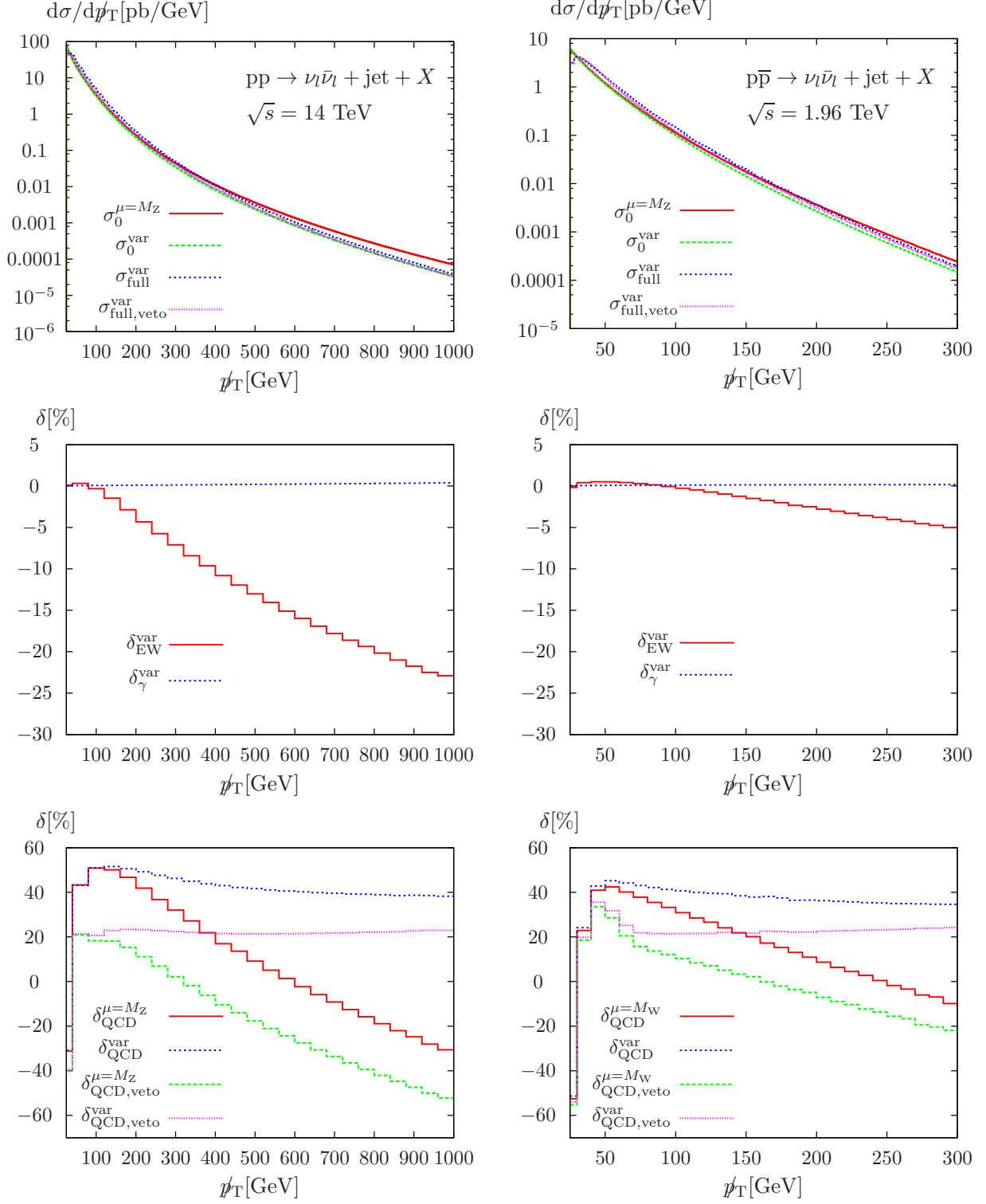


**Figure 8:** LO and fully corrected distribution (top), corresponding relative EW and photon-induced corrections (middle), and relative QCD corrections (bottom) for the missing transverse momentum at the LHC (left) and the Tevatron (right).

they matter most. However, any difference directly impacts the determination of the monojet cross section if a measurement of the  $l^+l^- + \text{jet}$  cross section is rescaled using a theoretical prediction for the cross-section ratio.

An obvious difference between the charged-lepton final state in contrast to the neutrino final state is the presence of final-state radiation (FSR). FSR is often modelled in the experimental analysis using shower techniques so that the bulk of this difference is assumed to be taken care of. Here, we want to focus on the remaining difference, which is not related to FSR, and matters at the 1% level. Hence, in the following, we compare  $\nu_l\bar{\nu}_l + \text{jet}$  production with  $l^+l^- + \text{jet}$  production without FSR, i.e. we subtract all photonic (QED) corrections to the  $Z \rightarrow l^+l^-$  decay, which correspond to a gauge-invariant subset of diagrams. The corresponding EW corrections are shown in Figure 9 for the distribution in the transverse momentum  $p_{T,V}$  of the vector boson and the transverse momentum  $p_{T,\text{jet}}$  of the leading jet at the LHC with a CM energy of  $\sqrt{s} = 8 \text{ TeV}$ , where  $p_{T,V} = p_T$  for the neutrino final state and  $p_{T,V} = p_{T,l^+l^-}$  for the charged-lepton final state. We use the variable scale (although not important for the relative EW corrections) and there is no visible influence of the treatment of photon–lepton recombination for the charged-lepton final state when FSR is subtracted.

At low transverse momenta, we observe an almost constant offset between the corrections to the different channels. The bulk of this offset can be attributed to the difference in the EW corrections to the partial widths of the different Z-boson decay modes, which are encoded in our calculation of the full EW corrections. While the corrections to the (on-shell)  $Z \rightarrow \nu_l\bar{\nu}_l$  partial width are roughly 0.9%, the weak corrections to the  $Z \rightarrow l^+l^-$  partial width (again subtracting the QED contribution) amount to  $-0.2\%$ .

Due to the universality of the Sudakov logarithms, one could expect the 1% offset, observed at small  $p_T$ , to be constant over the whole  $p_T$ -range. However, the EW corrections for the neutrino final state rise faster and are slightly larger in absolute size than their charged-lepton counterpart at  $p_T = 1 \text{ TeV}$ . This difference can be attributed to the photon-exchange contribution for the charged-lepton final state, which is part of the off-shell effects. For the EW correction in Figure 9, the event definition (see Ref. [24]) in this channel only asks for a dilepton invariant mass which is bigger than 50 GeV. In this case, the photon contribution is close to 10% for  $p_{T,V} = 1 \text{ TeV}$  (interference contributions are small). Since the Sudakov logarithms in the diagrams with an intermediate photon are much smaller (see Fig. 4 of Ref. [44]), the corrections for the charged-lepton final state are indeed smaller. For a tighter selection cut, asking for a dilepton mass close to the Z pole, the photon contribution is suppressed and the difference between the corrections in Figure 9 is indeed constant and almost completely due to the different corrections to the partial width, as shown in Figure 10. This dependence of the EW corrections in the Sudakov regime on the setup has to be taken into account at the 1–2% level, when using a measurement of the charged-lepton final state to predict the cross section for the monojet signature.

## 4 Combination of QCD and EW effects at NLO and beyond

In the discussion of our results in Section 3.3, we combined NLO QCD and EW corrections in a purely additive manner to present a full NLO prediction. Mixed EW×QCD corrections which are not part of the calculation are not addressed at all. Hence, the naive product of the NLO EW and QCD corrections represents an error estimate for higher-order corrections including EW effects.

This limitation is particularly important in the presence of improvements for the predictions on the QCD side: Parton-shower matching as well as dedicated resummations have become available, and even the calculation of next-to-next-to-leading-order QCD corrections might be

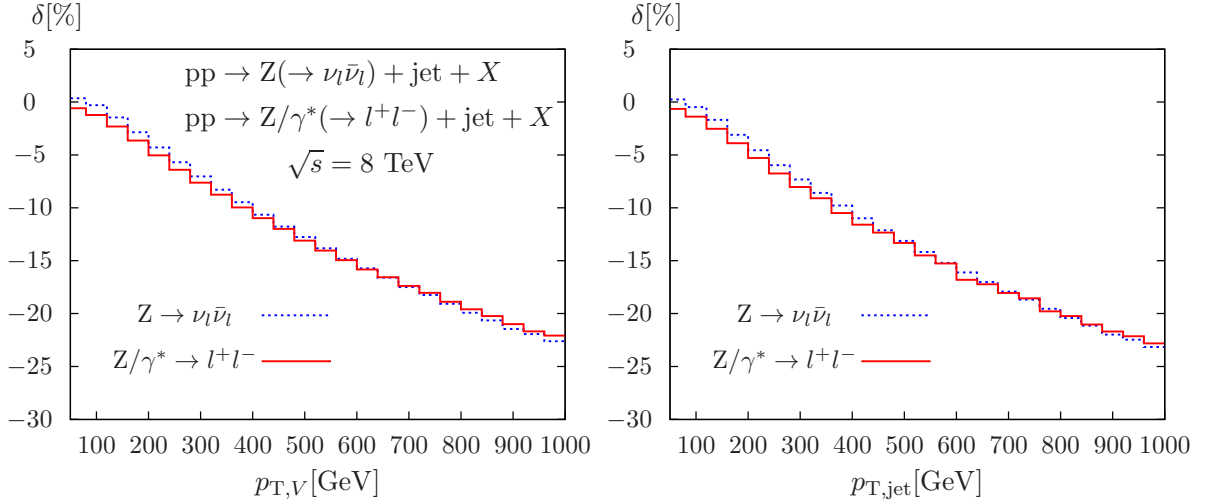


**Figure 9:** EW corrections (without final-state radiation) to the transverse-momentum distribution of the vector boson (left) and the leading jet (right) for the two different leptonic Z-boson decay modes,  $Z \rightarrow \nu_l \bar{\nu}_l$  and  $Z/\gamma^* \rightarrow l^+ l^-$ , in Z + jet production at the LHC ( $\sqrt{s} = 8 \text{ TeV}$ ).

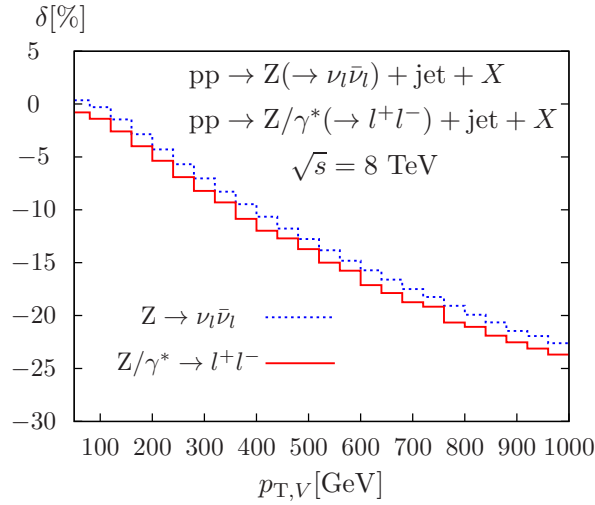


**Figure 10:** EW corrections (without final-state radiation) to the transverse-momentum distribution of the vector boson for the two different leptonic Z-boson decay modes,  $Z \rightarrow \nu_l \bar{\nu}_l$  and  $Z/\gamma^* \rightarrow l^+ l^-$ , in Z + jet production at the LHC ( $\sqrt{s} = 8 \text{ TeV}$ ). In contrast to the standard setup, a dilepton invariant-mass cut  $86 \text{ GeV} < M_{ll} < 96 \text{ GeV}$  is applied for the charged-lepton final state in order to suppress the  $\gamma^*$  component of the differential cross section.

within reach [45]. The increase in theoretical accuracy as well as the decreasing experimental errors at the LHC raise the question how to properly combine radiative EW corrections with the best available QCD prediction. In practice, a similar problem arises when EW corrections are to be included in “standard” QCD Monte Carlo tools.

Obviously, a completely satisfactory answer to this question can be found in the computation of the combined EW×QCD corrections, a very difficult task requiring involved two-loop calculations, which are beyond present computational possibilities. On the other hand, factorization of EW and QCD corrections is expected to be a good approximation. In fact, the large EW Sudakov logarithms, which completely dominate the EW corrections where they are most relevant, are part of the hard underlying production process. Therefore, it does not seem to be far fetched that there is not much interplay with soft and/or collinear physics dominating the QCD corrections.

The factorized ansatz for the EW×QCD corrections can, however, break down in certain kinematical situations and should, of course, not be applied blindly. A good example for such a breakdown is provided by the  $p_{T,\text{jet}}$  distribution in  $V + \text{jet}$  production. In Section 3.3, we have discussed that the tail of this distribution is completely dominated by back-to-back jets and does not contribute a generic NLO QCD correction to the LO kinematics. Applying the calculated EW corrections in a factorized form does not make any sense in this case. In fact, without a sensible jet veto, this work does not even supply a sensible estimate for the EW corrections for this observable at all. Only the calculation of the EW corrections to  $V + 2\text{jets}$  could improve the situation. Nevertheless, a dedicated jet veto solves the problem, and a factorized ansatz becomes a good approximation.

For other distributions, like the missing transverse momentum, the situation is fortunately simpler. The corresponding QCD corrections are uniform and moderate in size, as can be seen in Fig. 8, and one may safely assume a factorization of QCD and EW correction in this case, independent of a possible jet veto. Therefore, the best motivated prediction including EW corrections to the spectrum of the missing transverse momentum is given by

$$\frac{d\sigma_{\text{QCD}\times\text{EW}}^{\text{best}}}{d\cancel{p}_T} = [1 + \delta_{\text{EW}}(\cancel{p}_T)] \frac{d\sigma_{\text{QCD}}^{\text{best}}}{d\cancel{p}_T}, \quad (4.1)$$

with  $\delta_{\text{EW}}(\cancel{p}_T)$  taken from Fig. 8, where the best prediction available for the QCD-corrected cross section should be used. The residual uncertainties due to EW effects can then be estimated by the square of the relative EW corrections or equivalently by the two-loop EW high-energy logarithms [17]. A further reduction of EW uncertainties would require knowledge of the sub-leading higher-order logarithms, where potential cancellations between different logarithmic orders are expected.

The same reasoning also holds for the distributions in  $l^+l^- + \text{jet}$  production discussed in Ref. [24] or  $\nu_l l^+ + \text{jet}$  production discussed in Ref. [29]. Again, the calculated EW corrections to the  $p_{T,\text{jet}}$  distribution are only useful if an adequate jet veto is applied.

## 5 Conclusions

Following our study on  $l^-l^+ + \text{jet}$  production [24], we have presented the first calculation of the full NLO electroweak corrections to the production of one isolated hard jet at hadron colliders in the SM, which is an important signal process for various new-physics models. For all relevant observables the cross section is dominated by on-shell Z + jet production with a subsequent leptonic Z-boson decay. However, in our calculation all off-shell effects are taken into account.

We have implemented our results in a flexible Monte Carlo code which can model the experimental event definition at the NLO parton level. The separation of single-jet and single-photon production is consistently implemented by making use of the measured quark-to-photon fragmentation function. We have also recalculated the NLO QCD corrections supporting a phase-space-dependent scale choice. Photon-induced processes are included at leading order, but turn out to be phenomenologically unimportant.

The presented electroweak corrections to the total cross sections are at the permille level and are therefore negligible. Only in the tails of distributions, which are dominated by large centre-of-mass energies, the well-known Sudakov logarithms become dominant, and the electroweak corrections increase up to  $-25\%$  at transverse momenta of  $\sim 1$  TeV. For the  $p_{T,\text{jet}}$  and  $\cancel{p}_T$  distributions the results at large transverse momenta are in good agreement with earlier results for the  $l^+l^- + \text{jet}$  final state [24] as well as results obtained in the on-shell approximation for the Z boson [17].

The QCD corrections are moderate for observables that are dominated by transverse momenta below about 100 GeV. However, they can become extremely large (hundreds of percent) at jet transverse momenta  $p_{T,\text{jet}}$  of some 100 GeV unless a sensible veto on a second hard jet is applied. For the  $p_{T,\text{jet}}$  distribution, we have discussed that such a jet veto is essential for the applicability of the presented EW corrections. In contrast, the  $\cancel{p}_T$  distribution is quite stable against QCD corrections. Introducing a dynamical scale flattens the  $K$ -factor in the high-energy tails of the transverse-momentum distributions.

## Acknowledgements

This work is supported in part by the Gottfried Wilhelm Leibniz programme of the Deutsche Forschungsgemeinschaft (DFG) and by the DFG Sonderforschungsbereich/Transregio 9 ‘‘Computergestutzte Theoretische Teilchenphysik’’.

## References

- [1] N. Arkani-Hamed, S. Dimopoulos and G. R. Dvali, Phys. Lett. **B429** (1998) 263-272. [hep-ph/9803315].
- [2] S. Karg, M. Krämer, Q. Li and D. Zeppenfeld, Phys. Rev. D **81** (2010) 094036 [arXiv:0911.5095 [hep-ph]].
- [3] S. Karg *et al.*, PoS RADCOR **2009** (2010) 006.
- [4] H. Georgi, Phys. Rev. Lett. **98** (2007) 221601. [hep-ph/0703260].
- [5] B. Betz *et al.*, hep-ph/0606193.
- [6] T. G. Rizzo, Phys. Lett. **B665** (2008) 361-368. [arXiv:0805.0281 [hep-ph]].
- [7] G. Aad *et al.* [ATLAS Collaboration], Phys. Lett. B **705** (2011) 294 [arXiv:1106.5327 [hep-ex]].
- [8] S. Chatrchyan *et al.* [CMS Collaboration], Phys. Rev. Lett. **107** (2011) 201804 [arXiv:1106.4775 [hep-ex]] and JHEP **1209** (2012) 094 [arXiv:1206.5663 [hep-ex]].
- [9] L. Vacavant and I. Hinchliffe, J. Phys. G **G27** (2001) 1839-1850.

- [10] L. Benucci, [for the CMS Collaboration], PoS **HCP2009** (2009) 065. [arXiv:1001.5428 [physics.ins-det]].
- [11] W. T. Giele, E. W. N. Glover and D. A. Kosower, Nucl. Phys. B **403** (1993) 633 [hep-ph/9302225].
- [12] J. M. Campbell and R. K. Ellis, Phys. Rev. D **65** (2002) 113007 [hep-ph/0202176].
- [13] J. J. van der Bij and E. W. N. Glover, Nucl. Phys. B **313** (1989) 237.
- [14] S. Alioli, P. Nason, C. Oleari and E. Re, JHEP **1101** (2011) 095 [arXiv:1009.5594 [hep-ph]].
- [15] T. Becher, C. Lorentzen and M. D. Schwartz, Phys. Rev. Lett. **108** (2012) 012001 [arXiv:1106.4310 [hep-ph]].
- [16] J. H. Kühn, A. Kulesza, S. Pozzorini and M. Schulze, Phys. Lett. B **609** (2005) 277 [hep-ph/0408308].
- [17] J. H. Kühn, A. Kulesza, S. Pozzorini and M. Schulze, Nucl. Phys. B **727** (2005) 368 [hep-ph/0507178].
- [18] P. Ciafaloni and D. Comelli, Phys. Lett. B **446** (1999) 278 [hep-ph/9809321];  
V. S. Fadin, L. N. Lipatov, A. D. Martin and M. Melles, Phys. Rev. D **61** (2000) 094002 [hep-ph/9910338];  
A. Denner and S. Pozzorini, Eur. Phys. J. C **18** (2001) 461 [hep-ph/0010201];  
W. Beenakker and A. Werthenbach, Nucl. Phys. B **630** (2002) 3 [hep-ph/0112030];  
A. Denner, M. Melles and S. Pozzorini, Nucl. Phys. B **662** (2003) 299 [hep-ph/0301241].
- [19] G. Aad *et al.* [ATLAS Collaboration], Phys. Rev. D **85** (2012) 032009 [arXiv:1111.2690 [hep-ex]].
- [20] S. Chatrchyan *et al.* [CMS Collaboration], Phys. Rev. D **85** (2012) 032002 [arXiv:1110.4973 [hep-ex]].
- [21] H. Ita *et al.*, Phys. Rev. D **85** (2012) 031501 [arXiv:1108.2229 [hep-ph]].
- [22] G. Watt, JHEP **1109** (2011) 069 [arXiv:1106.5788 [hep-ph]].
- [23] A. Denner, S. Dittmaier, M. Roth and L. H. Wieders, Nucl. Phys. B **724** (2005) 247 [hep-ph/0505042];  
A. Denner and S. Dittmaier, Nucl. Phys. Proc. Suppl. **160** (2006) 22 [hep-ph/0605312].
- [24] A. Denner, S. Dittmaier, T. Kasprzik and A. Mück, JHEP **1106** (2011) 069. [arXiv:1103.0914 [hep-ph]].
- [25] A. D. Martin, R. G. Roberts, W. J. Stirling and R. S. Thorne, Eur. Phys. J. C **39** (2005) 155 [hep-ph/0411040].
- [26] J. Küblbeck, M. Böhm and A. Denner, Comput. Phys. Commun. **60** (1990) 165;  
H. Eck and J. Küblbeck, *Guide to FeynArts 1.0*, University of Würzburg, 1992;  
T. Hahn, Comput. Phys. Commun. **140** (2001) 418 [hep-ph/0012260].
- [27] E. Accomando, A. Denner and C. Meier, Eur. Phys. J. C **47** (2006) 125 [hep-ph/0509234].
- [28] T. Hahn and M. Pérez-Victoria, Comput. Phys. Commun. **118** (1999) 153 [hep-ph/9807565].

- [29] A. Denner, S. Dittmaier, T. Kasprzik and A. Mück, *JHEP* **0908** (2009) 075. [arXiv:0906.1656 [hep-ph]].
- [30] G. Passarino and M. Veltman, *Nucl. Phys. B* **160** (1979) 151;  
A. Denner and S. Dittmaier, *Nucl. Phys. B* **658** (2003) 175 [hep-ph/0212259] and *Nucl. Phys. B* **734** (2006) 62 [hep-ph/0509141].
- [31] G. 't Hooft and M. Veltman, *Nucl. Phys. B* **153** (1979) 365;  
W. Beenakker and A. Denner, *Nucl. Phys. B* **338** (1990) 349;  
A. Denner and S. Dittmaier, *Nucl. Phys. B* **844** (2011) 199 [arXiv:1005.2076 [hep-ph]].
- [32] S. Dittmaier, *Nucl. Phys. B* **565** (2000) 69 [hep-ph/9904440].
- [33] S. Dittmaier, A. Kabelschacht and T. Kasprzik, *Nucl. Phys. B* **800** (2008) 146 [arXiv:0802.1405 [hep-ph]].
- [34] A. Denner, S. Dittmaier, T. Gehrmann and C. Kurz, *Nucl. Phys.* **B836** (2010) 37 [arXiv:1003.0986 [hep-ph]].
- [35] E. W. N. Glover and A. G. Morgan, *Z. Phys. C* **62** (1994) 311.
- [36] D. Buskulic *et al.* [ALEPH Collaboration], *Z. Phys. C* **69** (1996) 365.
- [37] C. Amsler *et al.* [Particle Data Group], *Phys. Lett. B* **667** (2008) 1.
- [38] D. Y. Bardin, A. Leike, T. Riemann and M. Sachwitz, *Phys. Lett. B* **206** (1988) 539.
- [39] A. D. Martin *et al.*, *Eur. Phys. J. C* **63**, (2009) 189 [arXiv:0901.0002 [hep-ph]].
- [40] M. R. Whalley, D. Bourilkov and R. C. Group, in *HERA and the LHC*, eds. A. de Roeck and H. Jung (CERN-2005-014, Geneva, 2005), p. 575, hep-ph/0508110.
- [41] C. W. Bauer and B. O. Lange, arXiv:0905.4739 [hep-ph].
- [42] G. C. Blazey *et al.*, in *QCD and Weak Boson Physics in Run II*, eds. U. Baur, R.K. Ellis and D. Zeppenfeld (Fermilab-Pub-00/297, Fermilab, 2000) p. 47, hep-ex/0005012.
- [43] M. Cacciari, G. P. Salam and G. Soyez, *JHEP* **0804** (2008) 063 [arXiv:0802.1189 [hep-ph]].
- [44] J. H. Kühn, A. Kulesza, S. Pozzorini and M. Schulze, *JHEP* **0603** (2006) 059 [hep-ph/0508253].
- [45] A. Gehrmann-De Ridder, T. Gehrmann and M. Ritzmann, *JHEP* **1210** (2012) 047 [arXiv:1207.5779 [hep-ph]];  
T. Gehrmann and L. Tancredi, *JHEP* **1202** (2012) 004 [arXiv:1112.1531];  
A. Daleo, T. Gehrmann and D. Maitre, *JHEP* **0704** (2007) 016 [hep-ph/0612257];  
L. W. Garland *et al.*, *Nucl. Phys. B* **627** (2002) 107 [hep-ph/0112081] and *Nucl. Phys. B* **642** (2002) 227 [hep-ph/0206067].